Proceedings
1999 ASME International Mechanical Engineering Congress and Exposition
November 1999, Nashville, TN

STUDY OF EDGE EFFECTS IN LASER BENDING

Jiangcheng Bao and Y. Lawrence Yao*
Department of Mechanical Engineering, Columbia University
New York, New York 10027

ABSTRACT

Laser forming has not been widely used due to limited understanding of its mechanism and immaturity of processing technology. In the study of single axis laser bending of plates, edge effects affect accuracy of the bending. Experimental and numerical studies are carried out to study the mechanism of the edge effects. Temperature dependency of material properties and strain-rate dependency of yield stress are considered in numerical simulation. Numerical results match well with experimental results. Patterns of edge effects are examined in terms of bending angle variation and curved bending edge under different conditions. A more complete explanation for the mechanism of the edge effects is given.

1. INTRODUCTION

Laser forming, a new technique to induce controlled thermal deformation into components with laser, originates from the traditional sheet metal forming method -- flame bending, where the sheet metal is heated and deformed by an oxy-acetylene torch. More attention has been paid to laser forming in the past few years (Magee, et al., 1998). Laser forming involves heating the metal workpiece along a certain path with a defocused laser beam directed normal to the surface, and with or without a jet stream of cold gas or water emulsion cooling the path after the beam passes. During laser forming, a transient temperature field is caused by the irradiation and travelling of a laser beam. Consequently, thermal expansion and contraction take place, which give rise to deformation of the workpiece.

Laser forming has the following advantages over the traditional metal forming technologies: without any tools or external forces involved in the process, the cost of the forming process is greatly reduced when compared with traditional mechanical forming, especially for small batch and high variety of sheet metal components; with high flexibility of laser beam delivering system and power regulating system, it is much easier to incorporate laser forming into an automatic manufacturing system; material degradation in laser forming is limited to a very tiny area due to highly concentrated beam power.

Efforts have been made to understand the underlying mechanism in laser forming. F. Vollertsen (1994b) suggested that three kinds of mechanism may exist in laser forming, namely temperature gradient mechanism (TGM), buckling mechanism (BM) and upsetting mechanism (UM). TGM is dominant under conditions corresponding to a small Fourier number ($Fo = \alpha \cdot t/s^2$, where α is thermal diffusivity, t characteristic time and s sheet thickness) or modified Fourier number ($Fo = \alpha \cdot d/(s^2 \cdot v)$, where d is beam diameter at the workpiece surface and v traveling velocity). BM dominates for a high Fourier number. Two characteristics of this mechanism are no steep temperature gradient along the sheet thickness direction and the extension of heated area compared to the sheet thickness. UM is based on the increase of the sheet thickness and shortening of the sheet length. It is similar to BM while the dimension of the heated area is much larger than that in BM. Most research work to date has been focused on straight line laser bending.

Analytical models have been derived to predict the bending angle in the straight line laser bending. A simple beam model is proposed for TGM and an energy approach to the temperature field is assumed in Vollertsen's two layer model (Vollertsen, 1994a). In terms of agreement with experimental results, this model is a great improvement compared with previous analytical model. However, it assumes that all input energy is used for plastic deformation, and ignores the energy dissipation due to reversed straining during cooling. Mucha et al. (1997) has modeled TGM and provided solutions, by assuming different shaped plastic zones. This model assists with determining the critical conditions for TGM, but it can only be used to calculate the final bending angle, without any enlightening on the transient of the forming process, which is actually of great interest for understanding the underlying mechanism and realizing process control. By assuming a complete plastic zone in the area near the center of the beam, and a complete elastic zone in remote areas, Vollertsen et al. (1995) has established an analytical model for BM. This model is valid only for high ratio of thermal conductivity to thickness, i.e., the heat conduction procedure is completely a 2D case. This is, however, not always the case, especially when temperature gradient exists through the thickness direction.

To overcome the limitations of the analytical approach and generate more prediction capabilities, efforts have been made in numerical modeling. Alberti et al. (1994) carried out numerical simulation of the laser bending process by a coupled thermal mechanical analysis. Temperature dependency of flow stress was taken into consideration. Hsiao et al. (1997) simulated the bending process by taking into account the convection and radiation boundary condition, and using extrapolation for mechanical properties at higher temperature. Work hardening was not considered in Hsiao's model. Holzer et al. (1994) modeled the bending process under BM. An eight-node element was used, which is good for capturing the

* Contact: Y. Lawrence Yao, Department of Mechanical Engineering, Columbia University, 220 Mudd Bldg., MC4703, New York, NY 10027, Tel: (212) 854-2887, Fax: (212) 854-3304, Email: YLY1@columbia.edu

intensive temperature change, but not good for a bending-dominated deformation process such as laser bending. As temperature often rises to high levels in laser forming, temperature dependency of material properties becomes very important. Larger deformation is desired in laser forming, i.e., larger strain, and consequently, it is necessary to consider strain hardening, especially in the case of multiple scan (Sprenger, et al., 1994). In order to obtain higher productivity, high travelling velocities are often employed in laser forming. In such cases, the strain rate can go as high as 1.4 s^{-1}, and material properties show a great dependency on strain rate especially at elevated temperatures (Li and Yao, 1999).

Despite this progress, there still exist problems that need to be addressed before laser forming becomes a practical processing technology. Among them are the geometrical accuracy and mechanical properties of laser formed components. In the straight line laser bending, variation of the bending angle along the bending edge has been observed, as shown in Fig. 1 (b). The bending edge is also somewhat curved. These effects have been termed as edge effects which are obviously undesired since they cause the deviation from the desired constant bending angle along the bending edge as well as a certain warpage of the component, and may cause additional residual stresses, too.

Investigation (Magee, et al., 1997) has shown that the extent of edge effects depends on the thermal diffusion from the laser beam into the entire plate, and the geometrical constraints of the workpiece as it varies with distance from the end point of the scanning path. The actual profile of bending angle is dependent on the laser processing parameters employed, as well as the material properties. Materials with very different thermal conductivity and expansion exhibited different variation patterns of the bending angle. Attempts have been made to reduce edge effects by varying the traveling velocity empirically along the scanning path. Results showed that the varying velocity profile can lead to sizable reduction of the edge effects.

Theoretical analysis by Mucha et al. (1997) gives an analytical relationship between the bending angle and laser parameters, and describes the optimal conditions for forming. It also shows that thickness in the region around the bending edge has increased due to thermal contraction by TGM and the bending edge of the plate is visibly curved due to thermal contraction in the scanning direction. However, this analytical model calculates the bend angle at the end of process and does not describe the transient stages, while understanding of transient stages is useful for realizing process control.

This paper presents experimental and numerical investigations aimed at advancing the understanding of the mechanism of edge effects in straight line laser bending. Experimental results provide more laser forming data under different line energy and thickness. Numerical results provide more insights into the mechanism of edge effects, and help predict such effects on final dimensional accuracy and mechanical properties.

2. NUMERICAL SIMULATION

In this study, temperature and strain-rate dependency of material properties is considered. Work hardening, though less significant in single scanning, is also considered in order to improve simulation and prediction accuracy.

2.1 Assumptions

The following assumptions are made for the numerical modeling.

The power density distribution of the laser beam follows a Gaussian function. The laser operates in CW mode. No cooling gas or water jet is employed.

Material properties are temperature dependent, including thermal conductivity, specific heat, Young's modulus, Poisson ratio, and flow stress. Elastic strains are assumed to be much smaller than unity. The rate of deformation is the total strain rate, i.e., the sum of the elastic strain rate and plastic strain rate. Strain hardening of the material is considered by defining a strain hardening coefficient, which is also temperature dependent. Dependency of flow stress on strain rate is modeled by defining a stress ratio $R(\theta,\dot{\boldsymbol{\varepsilon}})$, the ratio of flow stress at a certain strain rate to the static flow stress, as a function of temperature θ and strain rate $\dot{\boldsymbol{\varepsilon}}$.

Dissipation of energy due to plastic deformation is negligible compared with the intensive energy involved. It is assumed that no melting is involved in the forming process.

2.2 Basic relationships

The effective laser beam diameter of the Gaussian distribution is defined as the diameter at which the power density decreases to $1/e^2$, i.e., the power within the circular area given by this diameter is 95% of the total power input. The basic equation of energy balance is

$$\int_V \rho \dot{U}\, dV = \int_S q\, dS + \int_V r\, dV \tag{1}$$

where V is the volume of a solid material with the surface area S, ρ the density of the material, $\dot{U}$ the material time rate of the internal energy, q the heat flux per unit area of the body flowing into the body, and r the heat supplied externally into the body per unit volume. By neglecting the coupling between mechanical and thermal problems, internal energy U is related to temperature θ by specific heat c:

$$c(\theta) = \frac{dU}{d\theta} \tag{2}$$

where c is the specific heat, θ the temperature of the material, U the internal energy of the material, which is dependent on the temperature only. Heat conduction is assumed to be governed by the Fourier law, i.e., heat flux is proportional to the temperature gradient, with thermal conductivity as the proportional constant.

The total strain is decomposed as follows:

$$d\boldsymbol{\varepsilon} = d\boldsymbol{\varepsilon}^{el} + d\boldsymbol{\varepsilon}^{pl} + d\boldsymbol{\varepsilon}^{c} + d\boldsymbol{\varepsilon}^{th} \tag{3}$$

where $\boldsymbol{\varepsilon}$ is total strain tensor, $\boldsymbol{\varepsilon}^{el}$ elastic strain tensor, $\boldsymbol{\varepsilon}^{pl}$ plastic strain tensor, $\boldsymbol{\varepsilon}^{c}$ creep strain tensor and $\boldsymbol{\varepsilon}^{th}$ thermal strain tensor. The thermal cycle in laser forming is very short, and is not repeated, so the effect of creep can be neglected. Assuming isotropic linear elasticity for metallic materials, the stress, $d\sigma$, can be expressed as:

$$d\sigma = Kd\varepsilon_{kk}\delta_{ij} + 2Gde_{ij} \tag{4}$$

where K is the bulk modulus and G the shear modulus, which can be computed readily from Young's modulus E and Poisson's ratio ν. Both Young's modulus E and Poisson's ratio ν are temperature dependent, and so are bulk modulus K and shear modulus G. Von Mises criterion is used as the yield criterion, which is a pressure

independent yield criterion. It takes the following form in isothermal state:

$$\frac{1}{6}\left[(\sigma_1-\sigma_2)^2+(\sigma_2-\sigma_3)^2+(\sigma_3-\sigma_1)^2\right]=K^2 \quad (5)$$

where σ_1, σ_2 and σ_3 are principal stresses. K is determined by a uniaxial experiment:

$$\frac{1}{3}\sigma_y^2=K^2 \quad (6)$$

where σ_y is the yield stress in the uniaxial tension experiment. For plastic deformation, the governing rule is the flow rule, which is given by:

$$d\boldsymbol{\varepsilon}=d\lambda\frac{\partial f}{\partial\boldsymbol{\sigma}} \quad (7)$$

where f is a function of $\boldsymbol{\sigma}$ that describes the yield criterion. With the Von Mises criterion, equation (7) becomes:

$$d\varepsilon_i=\frac{d\bar{\varepsilon}}{d\bar{\sigma}}\left[\frac{3}{2}\sigma_i-\frac{1}{2}\sigma_{kk}\right] \quad (8)$$

where $\bar{\varepsilon}$ is equivalent strain, $\bar{\sigma}$ is equivalent stress. Strain hardening describes the increase of yield stress with the accumulation of plastic deformation. In laser forming process, though every point of the workpiece experiences a thermal cycle, the mechanical loading, however, as far as the plastic deformation is concerned, is essentially monotonic. Thus, the isotropic hardening rule is adopted. With work hardening, the flow stress is related to strain by:

$$\sigma=K\cdot\varepsilon^n \quad (9)$$

where n is strain hardening coefficient, and can be found in literature. Strain-rate dependency of material properties is also taken into consideration by assuming that the flow stress is related with strain rate by the following equation:

$$\sigma=D\cdot\dot{\varepsilon}^m \quad (10)$$

where m is strain rate coefficient, and determined empirically (Li and Yao, 1999). For simplification, a ratio of yield stress to static yield stress, $R(\theta,\dot{\boldsymbol{\varepsilon}})$, as a function of temperature θ and strain rate $\dot{\varepsilon}$, is defined as:

$$R(\theta,\dot{\boldsymbol{\varepsilon}})=\bar{\sigma}/\sigma^0 \quad (11)$$

where $\bar{\sigma}$ is yield stress after considering strain rate, and σ^0 the static yield stress. The thermal strain $\boldsymbol{\varepsilon}^{th}$ is assumed to be related to a temperature matrix $\mathbf{T}$ by a linear coefficient of thermal expansion α. The energy balance model for deformation process follows:

$$\frac{d}{dt}\int_V(\rho\,\mathbf{v}\cdot\mathbf{v}/2+\rho U)\,dV=\int_S\mathbf{v}\cdot\mathbf{t}\,dS+\int_V\mathbf{f}\cdot\mathbf{v}\,dV \quad (12)$$

where ρ is the current density, $\mathbf{v}$ the speed field vector, U the internal energy per unit mass, $\mathbf{t}$ the surface traction vector, $\mathbf{f}$ the body force vector, $\mathbf{n}$ the normal of boundary S, V the volume in study, and S the corresponding boundary surface.

2.3 Numerical Schemes

Since the heat transfer and elastic/plastic deformation are symmetric about the vertical plane containing the scanning path, only half of the plate is modeled in the numerical simulation. The same mesh model is used for the heat transfer analysis and structural analysis. In order to capture high gradients of temperature near the scanning path, a fine mesh is used in that region, while a coarse one in remote areas.

A commercial code, ABAQUS, is used for the numerical simulation, using a sequentially coupled heat transfer and structural analysis. In structural analysis, the twenty-node element, C3D20, has no shear locking, no hourglass effect, and is thus suitable for a bending-deformation dominated process such as laser forming. On the other hand, the eight-node element suffers from "shear locking", and is therefore not suitable for such a process. In order to keep compatible with the structural analysis, a twenty-node element, DC3D20, is used in heat transfer analysis.

By standard Galerkin approach, equation (1) can be discretized in space:

$$\int_V N^N\rho\dot{U}\,dV+\int_V\frac{\partial N^N}{\partial\mathbf{x}}\cdot\mathbf{k}\cdot\frac{\partial\theta}{\partial\mathbf{x}}\,dV=\int_V N^N r\,dV+\int_{S_q}N^N q\,dS \quad (13)$$

where N is the nodal number. This set of equations is the "continuous time description" of the geometric approximation. With the backward difference algorithm

$$\dot{U}_{t+\Delta t}=\frac{U_{t+\Delta t}-U_t}{\Delta t}, \quad (14)$$

equation (13) can be discretized in time domain:

$$\frac{1}{\Delta t}\int_V N^N\rho(U_{t+\Delta t}-U_t)\,dV+\int_V\frac{\partial N^N}{\partial\mathbf{x}}\cdot\mathbf{k}\cdot\frac{\partial\theta}{\partial\mathbf{x}}\,dV=\int_V N^N r\,dV+\int_{S_q}N^N q\,dS \quad (15)$$

This nonlinear system is then solved by a Modified Newton method.

2.4 Boundary Conditions

The following boundary conditions are defined for the numerical simulation of the laser forming process.

Laser beam is given as prescribed nonuniform surface heat flux: $q = q(x, y, t)$ on the top surface. On five of the six boundary surfaces (except for the symmetric plane), free convection with air is considered: $q = h\,(\theta - \theta_0)$, where h is the heat transfer coefficient, and $\theta_0 = \theta_0\,(x, t)$ the surrounding temperature. Radiation is also considered on these five surfaces: $q = A((\theta - \theta_Z)^4 - (\theta_0 - \theta_Z)^4)$, where A is the radiation constant, and θ_Z the absolute zero on the temperature scale used. The symmetric plane is assumed to be adiabatic.

Two adjacent points in the middle of the symmetric plane are assumed to be fixed in order to remove the rigid body motion. All

other points within the symmetric plane are assumed to move only within the symmetric plane throughout the deformation process.

3. EXPERIMENT

A schematic of the straight line laser forming is shown in Fig. 1. Figure 1 (a) shows an ideal uniform bending angle α along the scanning path (defined as X axis). The bending edge along the X axis is not curved. The direction perpendicular to the scanning path and within the plate is Y axis. Figure 1 (b) is an actual deformed plate with a curved scanning edge and the bending angle α varies with x.

The laser machine used in the experiment is a PRC-1500 CO_2 laser, with a maximum output power of 1500 W. A Coordinate Measuring Machine (CMM) is used to measure the bending angle at different positions along the scanning path. Coordinates of different points along the scanning edge are also measured, and the curvature of the scanning edge is subsequently calculated from these coordinates.

Low carbon steel, AISI1010, is used in the experiment. Sheet size is 80 by 80 mm^2, and thickness is 0.60 mm and 0.89 mm. To enhance laser absorption by the workpiece, graphite coating is applied. A beam diameter of 8 mm is used in the experiment.

The experiment conditions are shown in Table 1.

Table 1 Experimental conditions

t (mm) / L.E.(J/mm)	0.60	0.89
20	P: 200 - 1300 W V: 10 - 67.5 mm/s	P: 200 - 1300 W V: 10 - 67.5 mm/s
30		P: 200 - 1300 W V: 6.7 - 45 mm/s

(t = thickness, L.E. = line energy)

By holding the line energy constant, the input energy per unit length along the scanning direction doesn't change, though the power and velocity do. The flatness of the unbent plates is measured using the CMM and the non-uniformity is smaller as compared with the final bending angle. A point clamp is used in the middle of one side of a workpiece (Fig. 1), as opposed to the line clamping reported in most publications. Using the point clamp, one can focus more on the edge-effects mechanism internal to the workpiece.

4. RESULTS AND DISCUSSION

Experimental results are presented first, followed by numerical results validated using the experiments. After additional numerical results are given, all the results are discussed together.

4.1 Experimental and Simulation Results

Figure 2 shows measurements of average bending angle vs. velocity with different line energy and thickness, with line energy held constant within each of the three groups. It can be seen from any groups in Fig. 2 that, despite the fact that the line energy is held constant, the average bending angle increases with velocity within the range of experimental conditions. Shown in Fig. 3 are measurements of curvature along X axis (scanning direction) vs. velocity with different line energy and thickness, with line energy held constant within each of the three groups. As seen, the curvature of workpiece along the scanning edge increases with the scanning velocity. Experimental results of variation of the bending angle along the scanning path are shown in Fig. 4. It can be seen that, from the entering end of the scanning path, the bending angle either drops a little and then increases or directly increases towards the exiting end, where the maximum value occurs. Experiments under other conditions (line energy = 20 J/mm for thickness = 0.89 mm and 0.60 mm) give similar results as in Fig. 4.

Figure 5 through 9 are comparison of numerical and experimental results to validate the numerical model. Shown in Fig. 5 is the variation of bending angle along the X direction at different velocities. Average bending angle and curvature vs. velocity are shown in Fig. 6 and Fig. 7, respectively. Figure 8 and Fig. 9 show bending angle variation and relative bending angle variation, respectively. The bending angle variation is defined as the difference between the maximal and minimal bending angle along the bending edge under a particular condition. The relative bending angle variation is defined as the ratio of the bending angle variation to the average bending angle. Generally speaking, there are good agreements between the experimental and simulation results. Not only the average bending angle and curvature, but also the bending angle variations along the scanning direction are relatively well captured by the numerical model.

Additional numerical results are shown in Fig. 10 through Fig. 13. The peak temperature that each point on the scanning path experienced is shown in Fig. 10. Apparently, the peak temperature at the entering end of the scanning path is much lower than that at the exiting end, while remaining largely constant at the rest of the scanning path. Figure 11 is the time history of temperature at the top and bottom surfaces along the scanning path for two different scanning velocities but at the same line energy. As seen, temperatures are higher at the higher velocity due to a shorter time for the heated workpiece to be exposed to environment and to conduct, and thus less energy dissipation. At the higher velocity, the difference between peak temperature at the top and bottom surfaces is also much larger than that at the lower velocity, which means the case at the lower velocity is more dominated by the Buckling Mechanism (BM) than the case with higher velocity. Figure 12 shows the simulation results of contractions in the X direction on the top and bottom surfaces along the scanning direction. Figure 13 shows the difference of the two contractions. The simulation result of bending edge curvature (Fig. 7) is also superposed here for the convenience of subsequent discussions.

4.2 Discussion

Despite the fact that the line energy is held constant, the average bending angle increases with velocity (Fig. 2). This is mainly due to the fact that, at higher velocities, temperatures are higher due to less energy dissipation and temperature difference between the top and bottom surfaces is greater (Fig. 11). The fact that the temperature at the exit point is much greater than that at the entrance point (Fig. 10) alone is sufficient to explain why the bending angle at the exit point is always greater than that at the entrance point (Figs. 4 and 5). This is a reason for the non-uniformity in the bending angle along the X axis.

It is well known that, in straight line laser bending, larger compressive plastic strain occurs near the upper layer in the Y direction and thickening occurs in the Z direction, both along the

scanning path. It is also known that compressive plastic strain occurs in the X direction as well. This is because during heating stage, thermal expansion in the X direction is greatly restricted just as in the Y direction, especially near the top surface where the temperature is higher and the material tends to expand (Fig. 11). But during cooling, the total contraction in the X direction near the bottom surface is greater than that on the top surface. This can be explained by the widely accepted assumption of constant volume (Mielnik, 1991):

$$d\varepsilon_1 + d\varepsilon_2 + d\varepsilon_3 = 0$$

where ε_1, ε_2 and ε_3 are strains in three mutually perpendicular directions. Under this assumption, the contraction in the Y direction near the top layer (which is required to form the bending angle) gives arise to a tendency of expansion in the X direction near the top layer, while the expansion in the Y direction near the bottom layer (which is also required to form the bending angle) will cause the bottom layer of the material to contract in the X direction. Therefore, the contraction near the bottom layer in the X direction is much larger than that near the top layer (Fig. 12). Consequently, the bending edge is curved away from the laser beam. The difference between the contractions near the top and bottom surfaces plotted in Fig. 13 correlates with the curvature of the bending edge very well. As seen, the greater the difference, the greater curvature.

Obviously, when the average bending angle is larger, the above mentioned effect will be more pronounced, and therefore the curvature will be greater. As seen from Figs. 2 and 3, at higher velocities where the average angles are larger, the curvatures of the bending edge are also greater.

But this is not the case for the bending angle variation shown in Fig. 8, where the variation, defined as the difference between the maximal and minimal bending angle along the scanning direction for a particular condition, rises quickly first, peaks at about 20 mm/s, and then levels off or slightly decreases with the increase of velocity. Please note that the curved bending edge and bending angle variation are related and they are together termed as the edge effects. Secondly, the increase of the curvature of the bending angle with the increase of velocity slows down at around 20 mm/s (Fig. 7). Therefore, it seems reasonable to conclude that the curved bending edge due to different contractions between the top and bottom surfaces is another reason for the bending angle variation along the scanning direction. The other reason is the temperature difference at the entrance and exit point as stated before.

5. CONCLUSIONS

Numerical results match with experimental results well. Not only the average bending angle and the curvature but also the bending angle variation can be reliably predicted. This is indicative of the reasonableness and comprehensiveness of the assumptions made in the numerical modeling for the conditions under which the investigation was carried out.

Both numerical and experimental results confirm that edge effects are characterized by a smaller angle at the entering end, and a largest angle at exiting end, as well as a curved bending edge for the conditions used in this paper. The same pattern holds for the different line energies and thicknesses investigated.

The bending angle variation is caused by the large temperature difference at the end points of the scanning path, as well as by the curving of the bending edge, while the curving is caused by the different contractions in the top and bottom layers of the plate in X direction.

6. ACKNOWLEDGEMENT

Financial support from Columbia University is gratefully acknowledged. Assistance by Dr. W. Li in strain rate consideration and experiments is also appreciated.

7. REFERENCE

Alberti, N., Fratini, L., Micari, F., "Numerical simulation of the laser bending process by a coupled thermal mechanical analysis," *Laser Assisted Net shape Engineering, Proceedings of the LANE'94*, Vol. 1, Meisenbach Bamberg, pp. 327-336.

Holzer, S., Arnet, H., Geiger, M., "Physical and numerical modeling of the buckling mechanism," ," *Laser Assisted Net shape Engineering, Proceedings of the LANE'94*, Vol. 1, Meisenbach Bamberg, pp. 379-386.

Li, W., Yao, Y. L., 1999, "Effects of strain rate in laser forming," submitted *to ASME Trans., J. Manufacturing Science and Engineering*.

Magee, J., Watkins, K. G., Steen, W. M., 1998, "Advances in laser forming," *Journal of Laser Applications*, Vol. 10 n 6, pp. 235-246.

Magee, J., Watkins, K. G., Steen, W. M., Calder, N., Sidhu, J. and Kirby, J., 1997, "Edge effects in laser forming," *Laser Assisted Net shape Engineering 2, Proceedings of the LANE'97*, Meisenbach Bamberg, pp. 399-408.

Mielnik, E. M., 1991, "Metalworking Science and Engineering," McGraw-Hill, Inc..

Mucha, Z., Hoffman, J., Kalita, W., Mucha, S., 1997, "Laser forming of Thick free plate," *Laser Assisted Net shape Engineering 2, Proceedings of the LANE'97*, Meisenbach Bamberg, pp. 383-392.

Sprenger, A., Vollertsen, F., Steen, W. M., Waltkins, K., 1994, "Influence of Strain Hardening on Laser Bending," *Laser Assisted Net shape Engineering, Proceedings of the LANE'94*, Vol. 1, Meisenbach Bamberg, pp. 361-370.

Vollertsen, F., 1994a, "An analytical model for laser bending," *Lasers in Engineering*, Vol 2, pp. 261-276.

Vollertsen, F., 1994b, "Mechanisms and models for laser forming," *Laser Assisted Net shape Engineering, Proceedings of the LANE'94*, Vol. 1, Meisenbach Bamberg, pp. 345 - 360.

Vollertsen, F., Komel, I., Kals, R., "The laser bending of steel foils for microparts by the buckling mechanism -- a model," Modeling and Simulation of Material Science and Engineering, Vol 3, pp. 107-119.

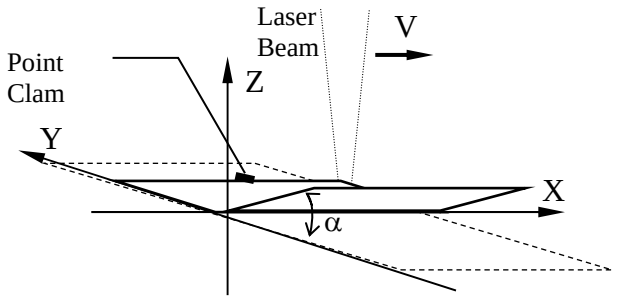

(a)

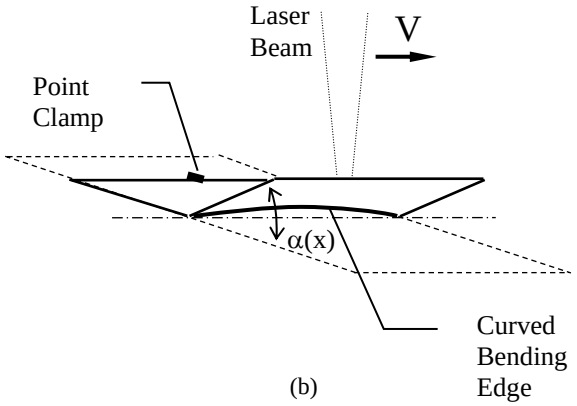

Fig. 1 Schematic of straight line laser bending
(a) showing no edge effects (b) showing edge effects characterized by the curved scanning edge and non-uniform bending angle varying along the scanning path $\alpha(x)$

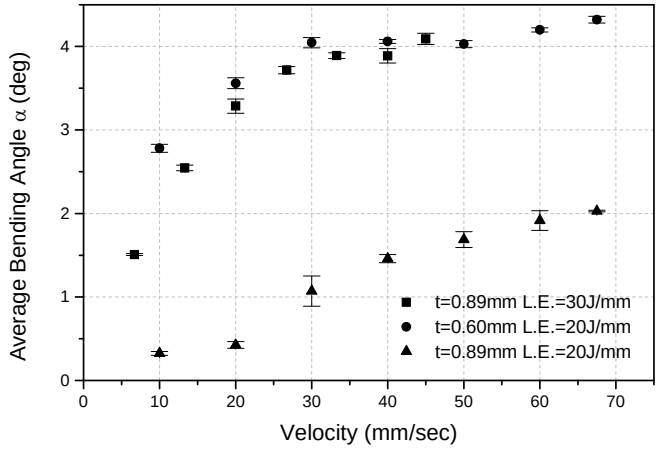

Fig. 2 Measurement of average bending angle at different velocity with line energy held constant (t = thickness, L.E.= line energy)

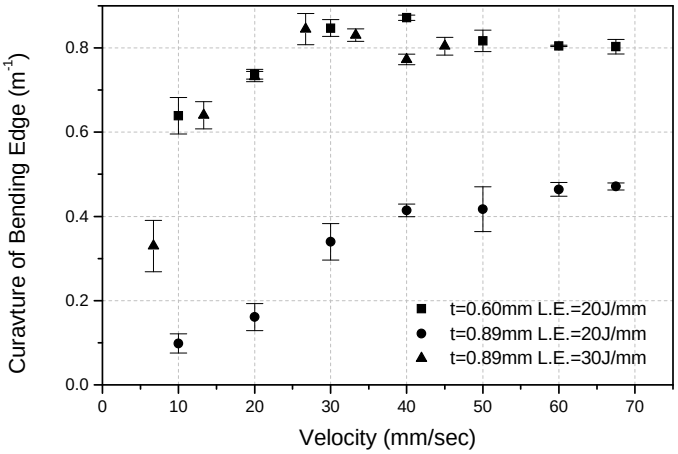

Fig. 3 Measurement of curvature of bending edge at different velocity with line energy held constant (t = thickness, L.E.= line energy)

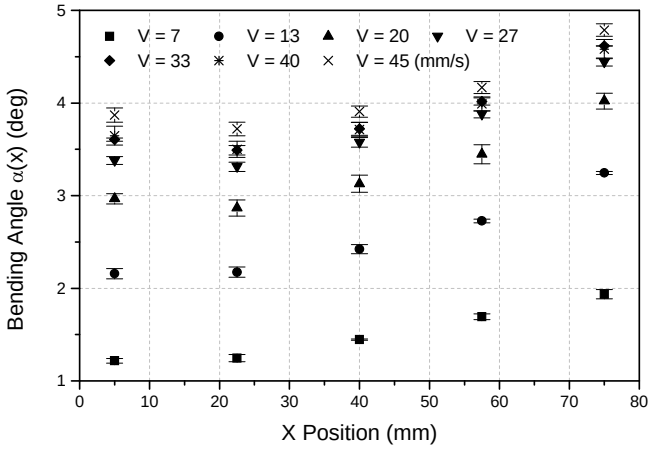

Fig. 4 Measurement of bending angle along the scanning direction (thickness = 0.89 mm, line energy = 30 J/mm)

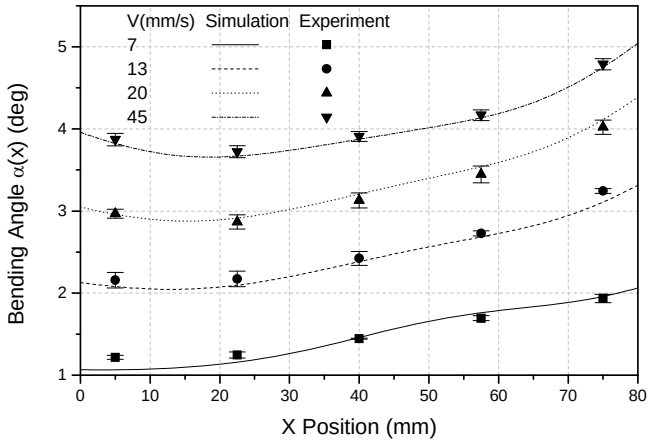

Fig. 5 Comparison of simulation and experiment -- bending angle $\alpha(x)$ (thickness = 0.89 mm , line energy = 30 J/mm)

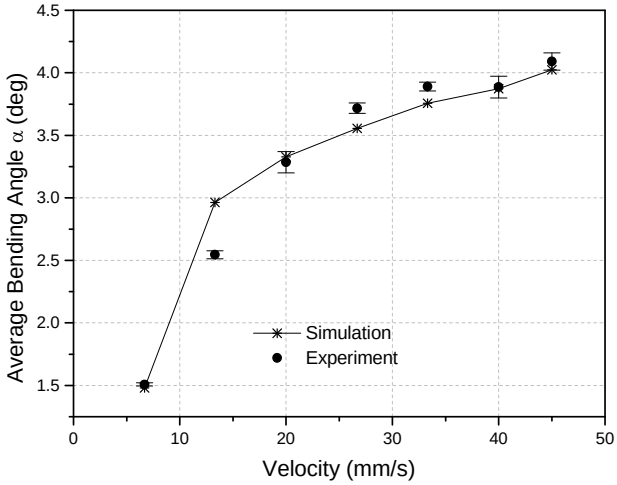

Fig. 6 Comparison of simulation and experiment -- average bending angle (thickness = 0.89 mm, line energy = 30 J/mm)

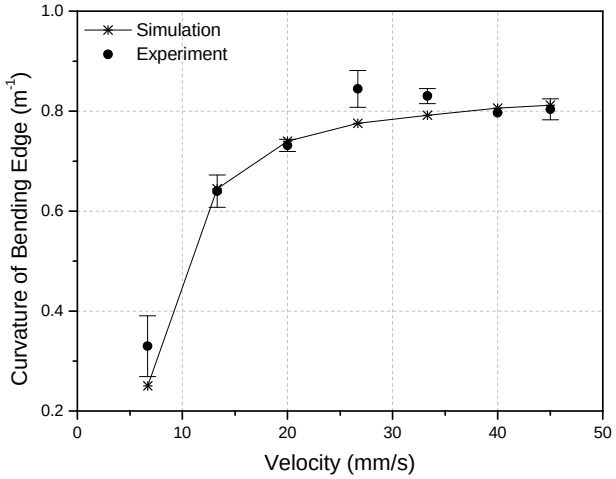

Fig. 7 Comparison of simulation and experiment -- curvature of the scanning edge (thickness = 0.89 mm, line energy = 30 J/mm)

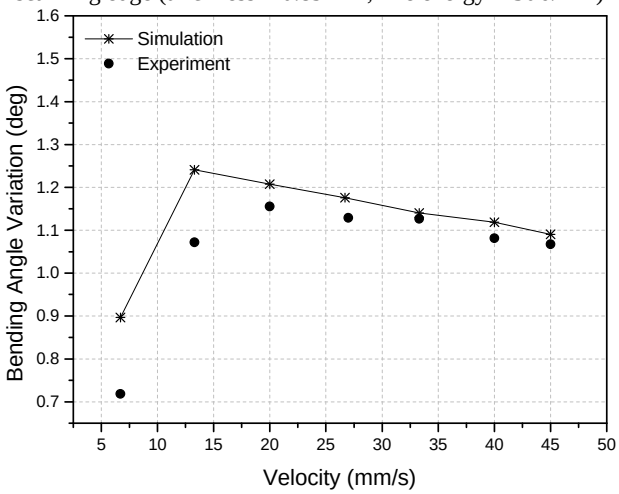

Fig. 8 Comparison of simulation and experiment -- edge effects (thickness = 0.89 mm, line energy = 30 J/mm)

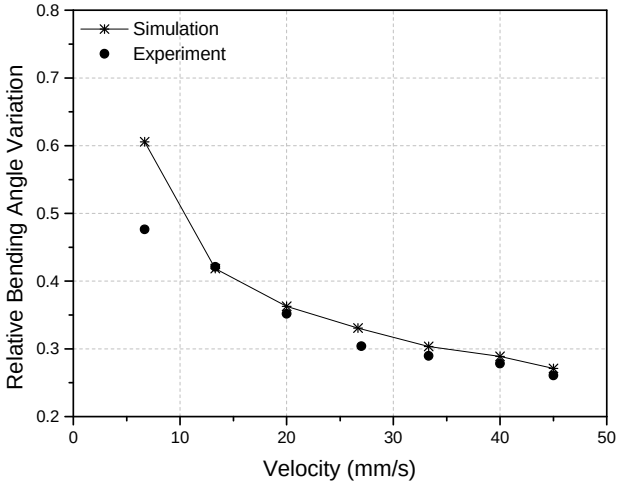

Fig. 9 Comparison of simulation and experiment -- relative bending angle variation (thickness = 0.89 mm, line energy = 30 J/mm)

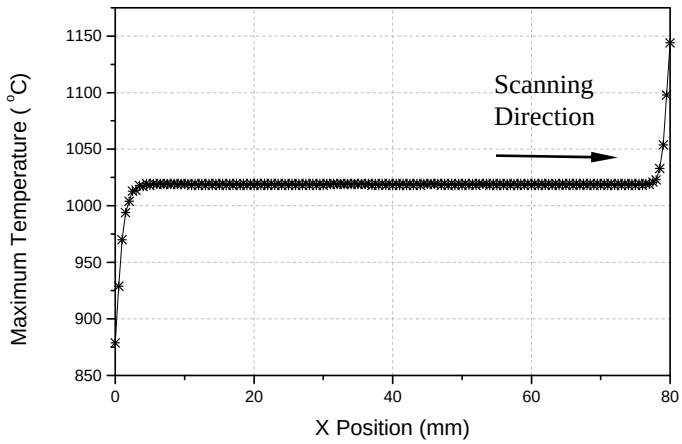

Fig. 10 Simulation results of maximum temperature along the scanning path
(thickness = 0.89 mm, line energy = 30 J/mm, velocity = 45 m/s)

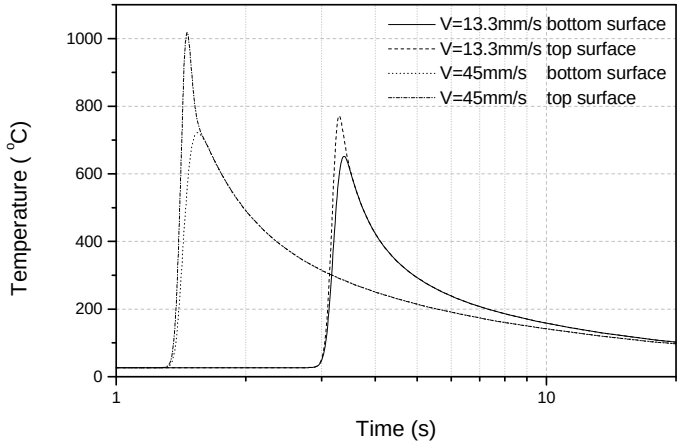

Fig. 11 Simulation results of temperature history on the scanning path
(thickness = 0.89 mm, line energy = 30 J/mm)

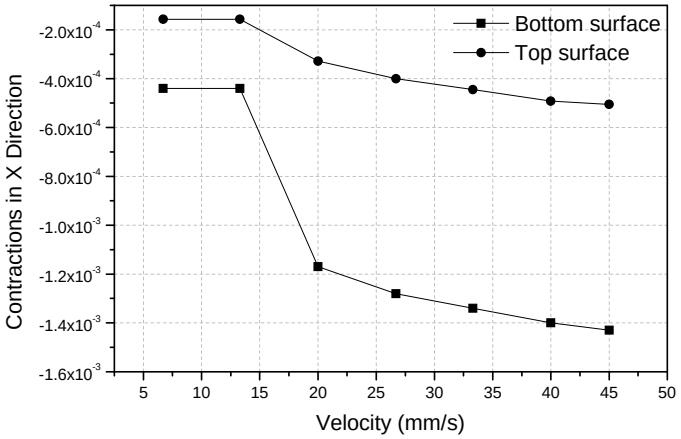

Fig. 12 Simulation results of contractions in X direction
(thickness = 0.89 mm, line energy = 30 J/mm)

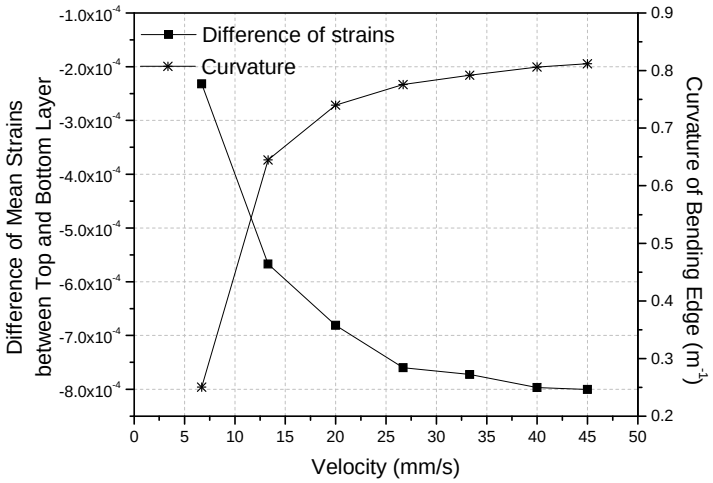

Fig. 13 Simulation results of difference of mean strains between top and bottom layer along the scanning direction (X axis) and curvature of the bending edge (thickness = 0.89 mm, line energy = 30 J/mm)